Journal of Colloid and Interface Science 650 (2023) 58–66

Contents lists available at ScienceDirect

Journal of Colloid And Interface Science

journal homepage: www.elsevier.com/locate/jcis

A Cytidine-Modified surfactant anchored liquid crystal Droplet-Based sensor for rapid and accurate detection of silver ions

Guannan Zhang, Wenting Zhao, Wenzhao Liu, Jun Zhou, Zhaoyang Wu *

State Key Laboratory of Chemo/Bio-sensing and Chemo-metrics, College of Chemistry and Chemical Engineering, Hunan University, Changsha 410082, People's Republic of China

GRAPHICAL ABSTRACT

Here, we synthesized a cytidine-based surfactant and anchored it onto the surface of liquid crystal (LC) droplets to enable the specific detection of silver ions. The synthesized surfactant could induce LC droplets into a radial configuration, and the introduction of silver ions changed the configuration of LC droplets in an intermediate (including escaped-radial and axial) configuration within 2 min. The LC droplet-based sensor developed here can specifically respond to the silver ions as low as 0.6 μM, making it suitable for the detection of Ag^+ in environmental and food samples.

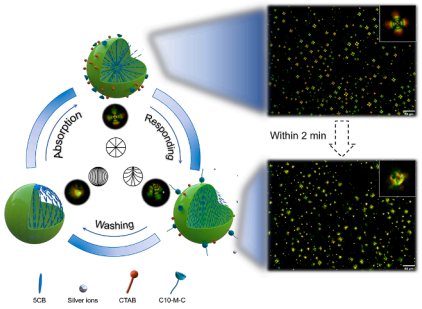

ARTICLE INFO

Keywords:
Liquid crystal droplet
Surfactant
Cytidine
Silver ion
Chemical sensor

ABSTRACT

Liquid crystal (LC) droplets exhibit unique and sensitive response behaviors to surface absorptions, making them promising candidates for sensing aplications. Here, we have developed a label-free, portable, and cost-effective sensor for the specific and rapid detection of silver ions (Ag^+) in drinking-water samples. To achieve this, we have modified cytidine into a surfactant (denoted as C10–M–C) and anchored it onto the surface of LC droplets. The specific binding ability between cytidine and Ag^+ enables LC droplets anchored with C10–M–C to respond rapidly and specifically to Ag^+ ions. Furthermore, the sensitivity of the response meets requirements for the harmless concentration of Ag^+ in drinking-water. The sensor we developed is label-free, portable, and cost-effectively. We believe that the sensor reported here can be applied to the detection of Ag^+ in drinking-water and environmental samples.

* Corresponding author.
E-mail address: zywu@hnu.edu.cn (Z. Wu).

https://doi.org/10.1016/j.jcis.2023.06.111
Received 5 April 2023; Received in revised form 12 June 2023; Accepted 16 June 2023
Available online 19 June 2023

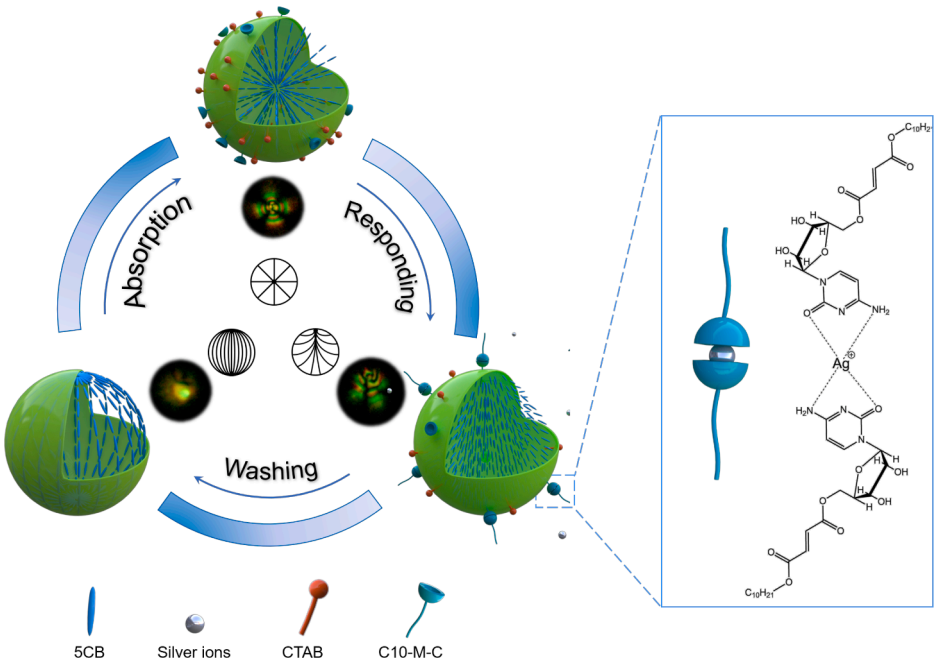

Fig. 1. Schematic diagram of the detection of silver ions using the LC droplet-based sensor.

1. Introduction

Silver ions have been widely used as potent antibacterial agents, as well as in the electronic manufacturing and pharmaceutical industries [1]. However, excessive discharge of silver ions into the environment can be toxic to various aquatic organisms, highlighting the need for a convenient and rapid strategy for monitoring silver ions. Existing methods for detecting silver ions mainly include fluorescent spectrum methods [2,3], electrochemical methods [4,5], and DNA-assisted colorimetric methods [6–8]. However, these approaches usually require sophisticated instrumentation or costly reagents. Therefore, a real-time, cost-effectively method for monitoring silver ions needs to be developed.

Liquid crystals (LCs) are materials that exhibit both the fluidity of a liquid and the anisotropy of a crystal. LC molecules show a rod-like rigid structure that imparts them with long-range ordered properties [9]. Stimulus arising from the absorption of analytes on the surface of LCs can be transitioned and amplified to changes of LC molecular arrangement at the micron level [10]. Various chemical and biological sensors had been developed based on the unique properties of LCs [11–13]. In particular, LC droplets-based sensors have emerged as a particularly promising platform due to their advantageous fluidic properties and high specific surface area, which confer upon them exceptional sensing capabilities [14–16].

LC droplets exhibit distinct birefringence patterns depending on the orientation of LC molecules within them. When LC molecules are oriented perpendicular to the droplet surface, which is known as the radial configuration, it shows a Malta-cross-like pattern under the polarizing microscope where there is a point defect located at the center of LC droplet. Conversely, when LC molecules are tangential to the droplet surface, which is referred to as the bipolar configuration and results in a full-moon-like pattern observed by the polarizing microscope where there are two point defects present at the poles of LC droplet [17]. Moreover, during the conversion between these two configurations, intermediate configurations such as axial, pre-radial, and escaped-radial configuration can arise [18]. During the configurational transition, defects can move from the center to the surface of the LC droplet or vice versa, accompanied by a change in the number of defects after undergoing an equatorial defect. Recently, several LC droplets sensors based on electrostatic interactions [19–22] and hydrophilic-hydrophobic interactions [23–25] have been developed. However, non-specific absorption resulting from these interactions between probes and targets can be easily interfered by similar reagents. Therefore, specific binding events on the surfaces of LC droplets need to be explored.

Here, we aimed to develop a novel LC droplet sensor for the specific detection of Ag^+ Fig. 1. Inspired by the specific binding interaction between cytosine and Ag^+ (C-Ag^+-C) [26], we have modified cytidine into a surfactant and used it as a probe to anchor onto the surface of LC droplets. The hydrophilic head of the cytidine group exhibited specific absorption of Ag^+, causing the surfactant desorption from the surface of LC droplet. Consequently, the configuration of LC droplets underwent a transformation, which was reflected in the altered birefringence patterns of LC droplets observed under a polarizing microscope. We believe this novel LC droplet sensor is expected to provide new sights for designing real-time outdoor chemical sensors.

2. Materials and experimental section

2.1. Materials and instruments

Materials: Acrylamide (AAm), ethylene glycol lipase, *n*-decyl alcohol, maleic anhydride, sodium acetate, *n*-Heptane, 4-methylbenzenesulfonic acid and silver nitrate solution (0.1 N in H_2O) was obtained from Shanghai Aladdin Bio-Chem Technology Co., Ltd. Cetyl trimethyl ammonium bromide (CTAB), N,N'-Methylenebisacrylamide (MBA), and 2-hydroxy-2-methylpropiophenone (HMPP) were purchased from Sigma-Aldrich. 4-cyano-4′-*n*-pentylbiphenyl (5CB) was purchased from Heibei Huajing Scientific and Technological Development Co., Ltd. N,*N*-Dimethylformamide (DMF), cytidine, lead dichloride, ferrous chloride tetrahydrate, copper dinitrate, mercury(II) nitrate monohydrate, zinc chloride, calcium chloride, chromium(III) citrate nonahydrate and nickel(II) chloride hexahydrate were obtained from Shanghai Titan Scientific Co., Ltd. All of the regents were of analytical purity. Ultrapure water (18.25 MΩ•cm) was obtained from ZOOMWO water purification system.

Instruments: Fourier Transform Infrared (FT-IR) measurements were performed on a Shimadzu IR Affinity-1 spectrometer. The ^1H NMR measurement was performed on Bruker AVANCE Neo 400 (400 MHz,

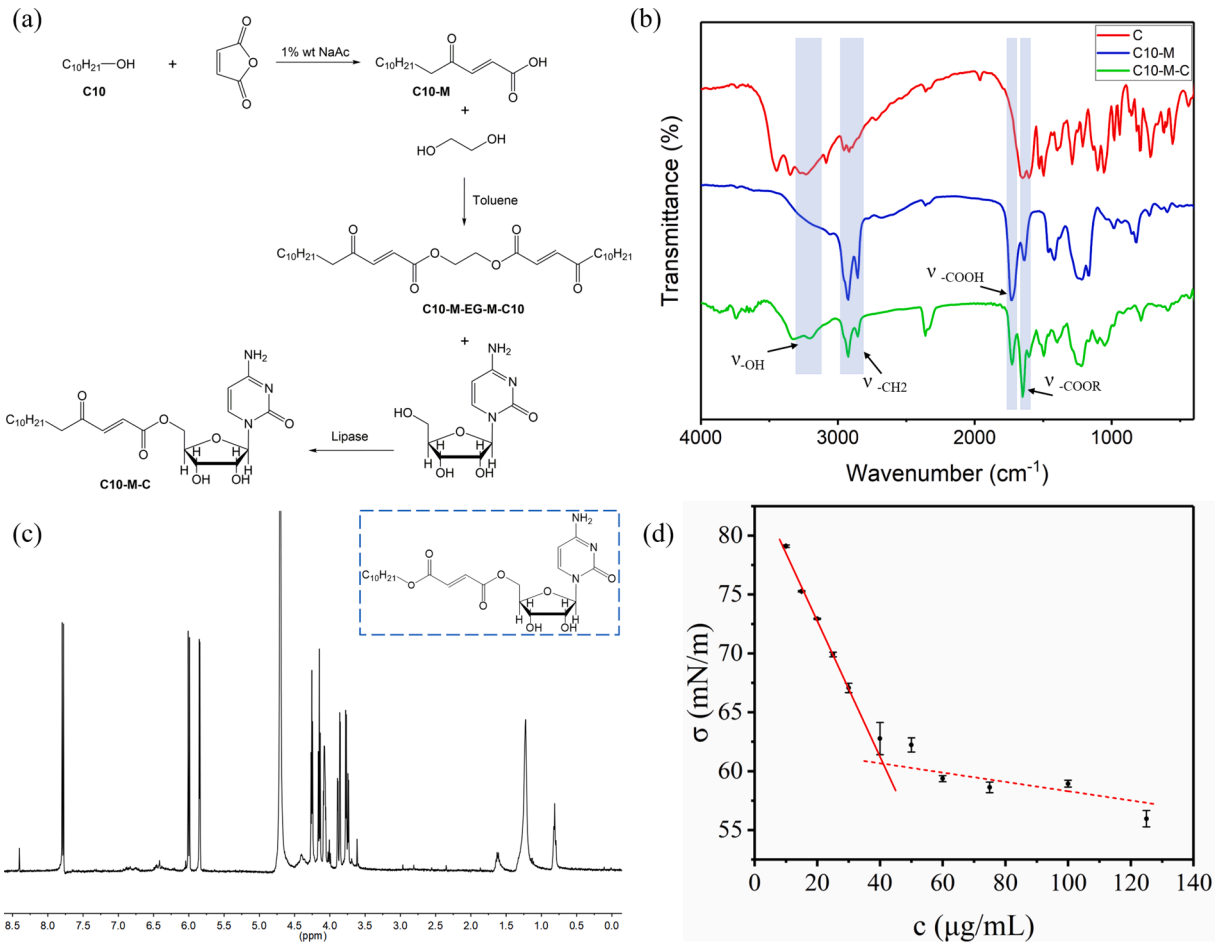

Fig. 2. (a) The synthesis route of C10–M–C. (b) The FT-IR spectrum and (c) the ^{1}H NMR.

German), and the sample was dissolved in D_2O. The optical appearance of LC droplets was observed with a polarizing optical microscope (Nikon ECLIPSE 50i POL, Japan) in a transmission mode, and optical microscopy images were acquired by a digital camera (MD50, Mshot, China). The interfacial tension of 5CB and surfactants solution was performed on LAUDA Scientific GmbH, LSA-100 (German). All glass slides used were treated with a plasma cleaner (PDC-36G, HF-Kejing Material Technology Co., Ltd., China).

2.2. General procedure for synthesis of C10–M–C

C10–M: The *n*-decyl alcohol (15.8 g, 0.1 mol), Maleic anhydride (9.8 g, 0.1 mol) and sodium acetate (0.256 g, 1 wt%) were added into a cleaning round-bottom flask and stirred at 80℃ for 3 h. After cooling to room temperature, the product was recrystallized using toluene to obtain white needle-like crystals.

C10–M–EG–M–C10: The C10–M (25.6 g, 0.1 mol) obtained above, ethylene glycol (3.1 g, 0.05 mol) and p-toluenesulfonic acid (0.029 g, 0.1 wt%) were dissolved in 100 mL toluene. The mixture was then stirred at 160℃ with removing water during a 6-hour period. After removing the solvent, the obtained product was washed with petroleum ether. The obtained yellow oily product was stored at room temperature for further use.

C10–M–C: The synthesis of C10–M–C was achieved through an enzymatic acylation. In detail, 65 mL heptane containing 26.9 g (50 mmol) C10–M–EG–M–C10 and 35 mL DMF containing 1.22 g (5 mmol) cytidine were mixed, and then 60 kU lipase was added to the mixture. The enzymatic acylation was carried out at 40℃ for 12 h. After removing the lipase and the solvent, the product was purified by column chromatography over silica gel using a gradient elution (eleuents: 20:1 MeOH- CH_2Cl_2 and 1:1 MeOH-CH_2Cl_2).

2.3. The preparation of PAAm hydrogel embedded with LC droplet-based sensor

The LC droplet-embedded PAAm hydrogel was prepared following our previous work. In detail, 25 μL 5CB was added to a precursor solution containing 0.1 g/mL AAm, 2.5 mg/mL MBA, 2.5 μL/mL HMPP and 1 mg/mL CTAB, then the mixture solution was dispersed into emulsion using a vortex stirrer (Mixer 4 K, Sangon Biotech Co., Ltd., Shanghai, China) at 4000 rpm. Next, the above emulsion was added to a home-made slide mold as shown in Figure S1. Immediately, the precursor solution in the slide mold was moved to a UV crosslinker (365 nm, 5 mW/cm^2, Scientz 03-II, Scientz Biotechnology CO., Ltd.) for 20 min. After washing by ethanol, PAAm hydrogels was immersed in 30% DMF solution for 12 h to remove the excess CTAB. Finally, LC droplets in PAAm hydrogel show a bipolar configuration and the PAAm hydrogels were stored at an aqueous solution for subsequently use.

2.4. The incubation of LC droplet-based sensor with CTAB and C10–M–C

To anchor the surfactant on the surface of LC droplets, PAAm hydrogels embedded with LC droplets were immersed in different concentration and ratio of CTAB and C10–M–C mixture solution at 40℃ for 10 min. Subsequently, the PAAm hydrogels were placed on a glass slide to observe LC droplets without under a polarizing microscope additional treatment.

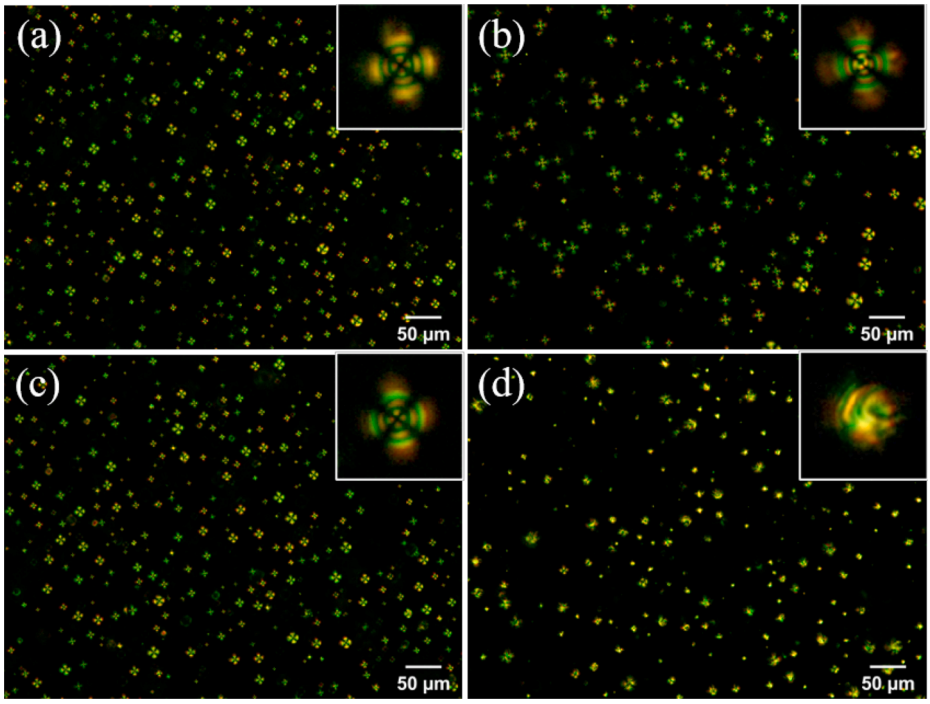

Fig. 3. Polarizing microscopy images of LC droplets embedded in PAAm hydrogel. (a) LC droplets with 10 mg/mL C10–M−C anchored on their surface; (b), (c), (d) correspond to LC droplets immersed in 1 mM NaOH, 1 mM HNO_3 and 10 μM $AgNO_3$, respectively, in the presence of 10 mg/mL C10–M–C.

2.5. Response of the LC droplet-based sensor to Ag^+ solution

Before responding to Ag^+ solution, PAAm hydrogels embedded with LC droplets were washed three times with water to remove excess CTAB and C10–M–C. Then the PAAm hydrogels were immersed in an Ag^+ solution of different concentrations for 2 min. Subsequently, the PAAm hydrogels were placed on a glass slide to observe LC droplets under a polarizing microscope without additional treatment.

2.6. The observation and counting of different configurations of LC droplets

The observation of LC droplets was achieve using a polarizing microscope under the orthogonal state. To counting different configurations of LC droplets, five regions at the center and corner of the hydrogel film were selected. Then different configuration of LC droplets was counted and their proportions were calculated.

2.7. Calculation of the surface coverage of surfactants on LC droplets.

The surface coverage of surfactants on LC droplets can be determined by measuring the interfacial tension between their solution and LC (5CB), followed by calculation using the equation provided below [27]:

$$\gamma - \gamma_0 = \Gamma_\infty RT[\ln(1-m)] - \frac{Km^2}{2}$$

where γ and γ_0 represent the interfacial tensions between LC and the surfactant solution, and between LC and water, respectively; R is the gas constant, and T is the absolute temperature; *m* denotes the surface coverage of surfactants on LC droplets, and Γ_∞ is the maximum adsorption capacity of the surfactant. The value of Γ_∞ for CTAB is 3.39 $\times$ 10^{-6} mol•m^{-2}, while the value of Γ_∞ for C10–M–C is calculated to be 4.19 $\times$ 10^{-4} mol•m^{-2} according to the previous report [28]. To simplify the calculation process, the value of K is set to 0. By converting all numerical values to standard units, the surface coverage (*m*) of surfactants on LC droplets can be determined.

2.8. Recyclability of LC droplet-based sensor

To regenerate the radial configuration of LC droplets after responding to Ag^+ solution, the hydrogel film embedded with LC droplets was first immersed in a 30% DMF solution for 12 h, with the solution being changed every 4 h. Then, CTAB and C10–M–C were re-anchored to the surface of LC droplets according to the method described in Section 2.4. At this point, the LC droplets can be reused for the detection of Ag^+ solution.

3. Results and discussion

3.1. The synthesis of cytidine-based surfactant C10–M–C

Enzymatic reactions have been highly appreciated in recent years due to their environmentally-friendliness, remarkable selectivity and exceptional efficiency. As a result, the modification of cytidine was achieved through the enzymatic acylation. The lipase can break the ester bond and specifically modify acyl group at the 5′ site of cytidine [29]. Thereby, we attempted to introduce an ester group on the dcyl alcohol (C10) at first (Fig. 2a). The introduce of ester group was achieved by linking ethylene glycol (EG) and *n*-decyl alcohol (C10) through the maleic anhydride (M). Resulting products were cleavage by lipase (obtained from the Aspergillus oryzae) and achieved the acylation of cytidine (C). Finally, the mixed products were separated by column chromatography, and the product (denoted as C10–M–C) was expected to be eluted as a highly polar component.

The synthesis of C10–M–C was confirmed by FT-IR and ^{1}H NMR spectrum. As shown in Fig. 2b, the C10–M–C show characteristic absorption peaks for hydroxyl and alkyl chains at 3220 cm^{-1} and 2920 cm^{-1}, respectively. Besides, a decrease in the absorption peak at 1730 cm^{-1} and an increase in the absorption peak at 1650 cm^{-1} was observed, which indicates that the esterification of carboxylic group in C10–M. Furthermore, the synthesis of C10–M–C can be also confirmed by ^{1}H NMR, where C10–M–C was dissolved in D_2O. As shown in Fig. 2c, the chemical shift of proton peaks at 7.79 ppm and 6.01 ppm implies that the presence of cytosine, while the peaks at 0.81 ppm and 1.23 ppm are

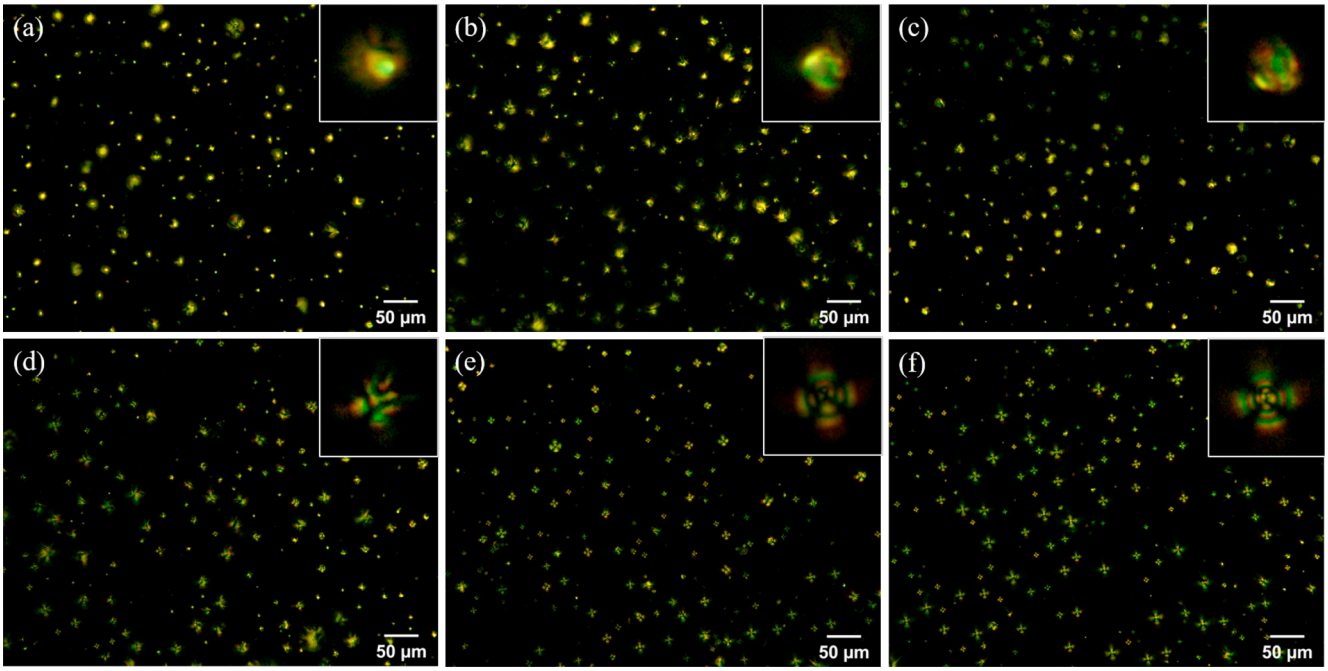

Fig. 4. The optimization of CTAB concentration in the mixture solution of CTAB and C10–M–C. The figure a-f refer to polarizing microscopy images of the PAAm hydrogel embedding with LC droplets immersed in a 0, 0.2, 0.4, 0.6, 0.8 and 1.0 μg/mL CTAB solution, respectively.

attributed to the alkyl chain of C10. These results demonstrate the successful synthesis of C10–M–C.

3.2. The surfactant nature of C10–M–C

Next, we present an analysis of the surfactant nature of C10–M–C, focusing on its HLB value and critical micelle concentration (CMC). The HLB value, a measure of the balance between hydrophilic and lipophilic parts of surfactant, plays a crucial role in determining its amphiphilic properties. Here, the calculation of HLB value for C10–M–C is 11.19 according to the Davies' method [30]. This value indicates that C10–M–C can be used to form oil-in-water (O/W) emulsions, which is also capable of dispersing the LC into droplets in an aqueous solution. Upon addition to an aqueous solution containing LC droplets, the C10–M–C adsorb onto the surface of droplets, exposing its cytidine group to aqueous phase while its alkyl chain extends into the interior of LC droplets. The CMC of C10–M–C was determined by measuring its surface tension. As shown in Fig. 2d, the CMC of C10–M–C is 41.05 μg/mL (86 μM). As the concentration of C10–M–C exceeds its CMC, the rate of decrease in surface tension slows down with the addition of C10–M–C. These results indicates that the C10–M–C shows good amphipathic.

3.3. The preparation of PAAm hydrogel embedded LC droplet-based sensor

Subsequently, we prepared LC droplets that were embedded in a polyacrylamide (PAAm) hydrogel using the method developed in our previous work [31]. After preparing the LC droplet-embedded PAAm hydrogel films following the steps outlined in section 2.3, the excess CTAB on LC droplet surface was eliminated using a 30% DMF solution. Only after removing the excess CTAB, were we able to anchor signal recognition molecules on the surface of LC droplets. As a result, LC droplets with bipolar configuration embedded in PAAm hydrogel were acquired.

3.4. The configuration of LC droplets induced by C10–M–C and the anchoring stability of C10–M–C on the LC droplets surface

Adsorption of surfactants onto the surface of LC droplets can induce LC molecules to orient perpendicular to the surface, balancing the surface anchoring energy and elastic free energy, resulting in a radial configuration. We thus tried to introduce C10–M–C to the surface of LC droplets and evaluate its stability upon adsorption. As illustrated in Fig. 3a, LC droplets exhibited a radial configuration after the hydrogel being immersed in a 10 mg/mL C10–M–C solution, indicating successful adsorption of C10–M–C onto the LC droplet surface. As a nonionic surfactant, the hydrophilic head of C10–M–C is less susceptible to acid and base effects. After immersing the hydrogel in a 1 mM NaOH (Fig. 3b) or a 1 mM HNO_3 (Fig. 3c) solution, LC droplets with C10–M–C anchored still exhibit a radial configuration, demonstrating that the stability of C10–M–C against acids and bases, and its ability to adsorb stably on the surface of LC droplets. In addition, cytidine can coordinate with Ag^+ specifically to form a "C-Ag^+-C" structure. When the hydrogel was immersed in a 10 μg/mL $AgNO_3$ solution, a transformation of LC droplets was occurred, as shown in Fig. 3d, indicating that the introduction of Ag^+ weaken the anchoring strength of C10–M–C on the LC droplet surface. Collectively, these results suggest that C10–M–C can serve as a well-performing signal transduction molecule for detecting Ag^+ in an LC sensor.

3.5. The optimization of CTAB and C10–M–C mixture solution

However, the radial configuration for LC droplets induced by C10–M–C alone requires a high concentration, which is not conducive to improving the sensitivity for Ag^+ detection. To overcome this limitation, we utilized a CTAB and C10–M–C mixture solution to adjust the configuration of LC droplets. The reason we chose CTAB as a component in the mixed solution is because CTAB has a relatively low concentration requirement for inducing LC configuration transition (Figure S2), while also considering cost-effectiveness. Nonetheless, a higher concentration of CTAB can disrupt configurational transition during the combination between C10–M–C and Ag^+. Therefore, we investigated the optimized concentration of CTAB at first. As seen in Fig. 4, the addition of CTAB

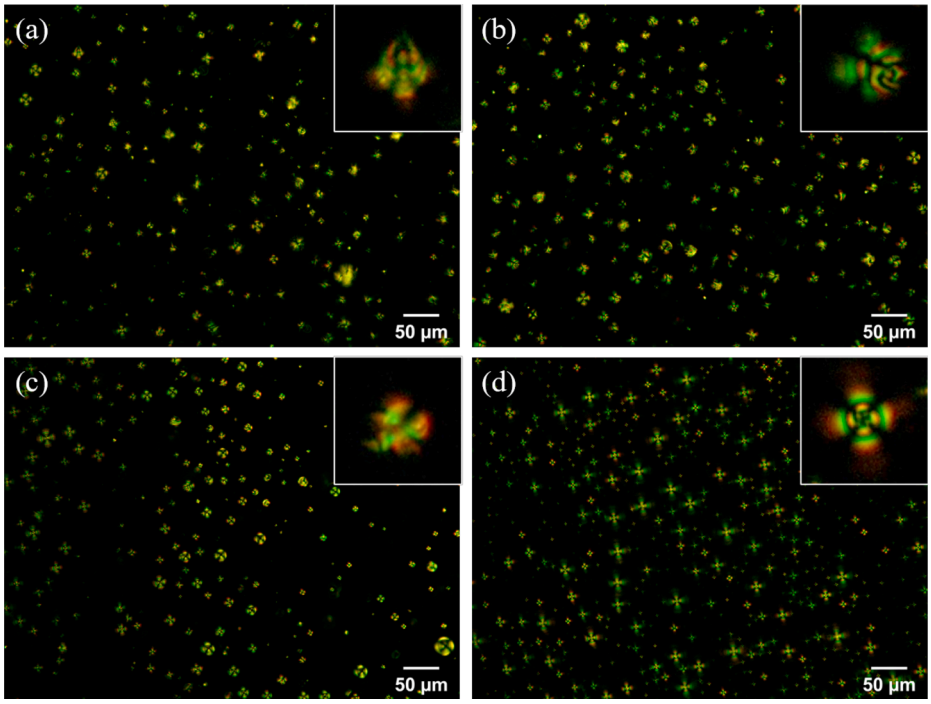

Fig. 5. The optimization of C10–M–C concentration in the mixture solution of CTAB and C10–M–C. The figure a-d depict polarizing microscopy images of PAAm hydrogel embedding with LC droplets immersed in a 0.4, 0.6, 0.8 and 1.0 μg/mL C10–M–C solution in the presence of 0.4 μg/mL CTAB, respectively.

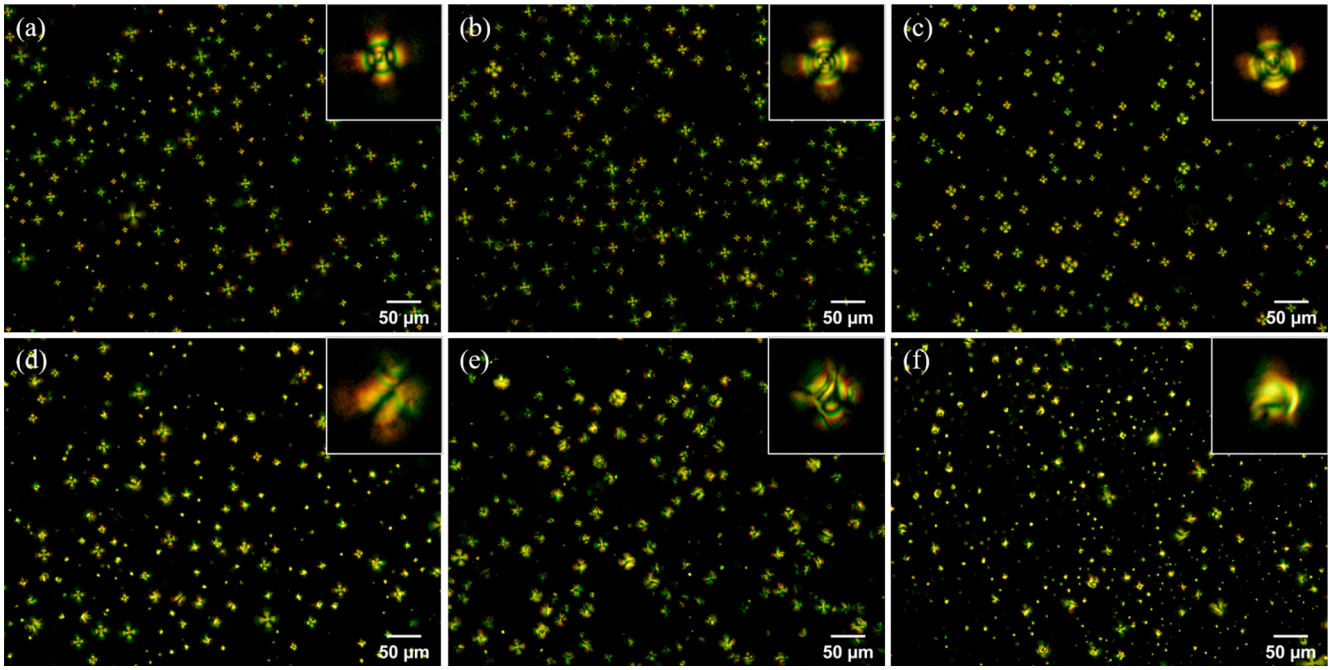

Fig. 6. The response sensitivity of LC droplet sensor to Ag^{+} generated by C10–M–C. Figure a-f show polarizing microscopy images of LC droplets in response to 0, 0.2, 0.4, 0.6, 0.8, 1.0 μM Ag^{+} solution after the incubation in a mixture solution of 0.4 μg/mL CTAB and 1.0 μg/mL C10–M–C.

triggered a configurational transition from bipolar to radial for LC droplets. The LC droplets exhibited intermediate and radial configurations at 0.6 μg/mL CTAB, whereas an intermediate configuration was observed when the concentration of CTAB is 0.4 μg/mL. Thus, the optimal concentration of CTAB in the mixture solution was determined as 0.4 μg/mL, at which the configuration of LC droplets was not disrupted. At this concentration, the surface coverage of CTAB on LC droplets is 79.24%, which will significantly reduce the concentration of C10–M–C required to induce LC droplets to adopt a radial configuration.

Subsequently, we optimized the ratio of C10–M–C and CTAB in mixture solution in the presence of 0.4 μg/mL CTAB. Polarizing microscopy images in Fig. 5 reveal that LC droplets exhibit a radial configuration completely upon the introduction of 1.0 μg/mL C10–M–C, suggesting that the optimal ratio for mixture solution is 0.4 μg/mL CTAB and 1.0 μg/mL C10–M–C. At this ratio, the surface coverage of the mixed surfactants on LC droplets is 90.29%, causing LC droplets to exhibit a

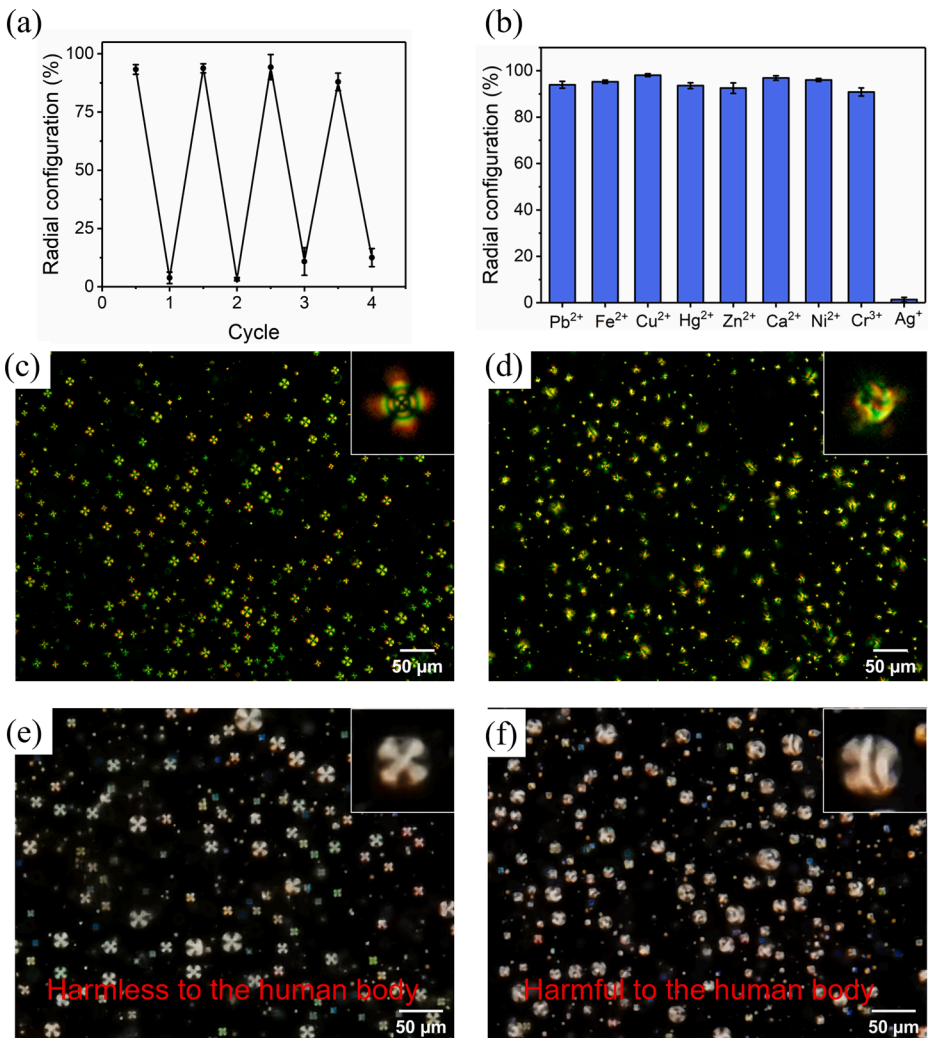

Fig. 7. (a) Reproducibility of the configuration of LC droplets. (b) Selectivity of LC droplet-based sensor response to metal ions. (c) and (d) represent the polarizing microscopy images of LC droplet-based sensor towards the river water sample with and without the addition of 1 μM Ag^+, respectively. (e) and (f) represent the polarizing microscopy images of LC droplet-based sensor towards the river water sample with and without the addition of 1 μM Ag^+, respectively, both captured directly using a smartphone.

radial configuration. Further experiments were conducted using the mixture solution with this determined ratio and concentration.

3.6. The sensitivity of LC droplet-based sensor towards Ag^+

Next, we investigated the response sensitivity of LC droplet-based sensor to Ag^+ generated by C10–M–C. As shown in Fig. 6, an increase in $AgNO_3$ concentration resulted in the transformation of LC droplets from radial to intermediate configuration. The intricate configuration of LC droplets is a result of a delicate balance between surface anchoring energy and elastic free energy [32] when there are no external fields. The introduction of Ag^+ leads to the formation of C-Ag^+-C structure, resulting in a decrease in the surface coverage of C10–M–C on LC droplets. Figure S3 demonstrates that upon the addition of 1 μM Ag^+, the interfacial tension between LC and the mixture solution increases, thereby reducing the surface coverage of mixed surfactants on LC droplets from 90.29% to 83.19%. Consequently, this decrease results in a reduction of the surface anchoring energy penalty. LC molecules in the droplets then redirect to reduce the elastic free energy, driving a transition in the configuration of LC droplets, which is visually apparent as changes in their patterns under the polarizing microscope (Fig. 6 d, e, and f). A significant transformation in configuration of LC droplets could be observed when the concentration of $AgNO_3$ reached 0.6 μM. According to the *Guidelines for Drinking-water Quality, Fourth Edition* from WHO, a human can tolerate up to 0.1 mg/L, or 0.93 μM Ag^+ without risk to health. Therefore, we conclude that the sensor reported here is capable of responding to Ag^+ as low as 0.6 μM, which meets the requirement for detection of Ag^+ in drinking-water samples.

3.7. The reusability of the LC droplet-based sensor

The ability to be used repeatedly is a crucial attribute of sensors. LC droplets are confined within the PAAm hydrogel, allowing for renewal of surface adsorption through simple washing procedures. Thus, the LC droplet-based sensor can be regenerated by washing it with 30% DMF solution and re-immersing the PAAm hydrogel embedding with LC droplets in the CTAB and C10–M–C mixture solution. Fig. 7a illustrates the reusability of the LC droplet-based sensor. The configuration of LC droplets exhibited good reproducibility with negligible volume loss of LC droplets during four cycle of washing and responding procedure (Figure S4 e and f), which indicates that the LC droplet-based sensor hold significant potential for practical applications due to its good recyclability.

3.8. The selectivity of LC droplet-based sensor to metal ions

The coordination between cytidine and Ag^+ is a specific interaction that permits LC droplets to selectively respond to Ag^+. Fig. 7b depicts that LC droplets anchored with C10–M–C showing negligible interference and remains in a radial configuration from other metal ions (Figure S5), demonstrating their potential for accurate and reliable detection of Ag^+ in complex samples.

Table 1
The comparison of different methods for Ag^+ detection.

Methods	Strategies	Sensitive of Detection	Signal readout mode	Reference
Localized Surface Plasmon Resonance (LSPR)	Reduce the SPR signal of AgNPs using carbon dots	26 nM	UV–visible spectrometry	[33]
Fluorescence	Using Ag^+ to modulate the fluorescence signal of CdSe quantum dots	70 nM	Fluorescence Spectroscopy	[34]
C-Ag^+-C mismatch in a C-rich ssDNA	Ag^+ competitively adsorb cytidine in the presence of methylene blue	58 nM	UV–visible spectrometry	[35]
Fluorescence	enhancement effect on the photoluminescence of C-dots generated by Ag^+	320 nM	Fluorescence Spectroscopy	[36]
colorimetry	Catalytic reduction of Ag^+ to the surface of AuNPs	1 μM	Naked eye	[37]
LC droplet-based sensor	Arginine-assisted liquid crystal droplets sensor	0.6 μM	Smartphone	This work

3.9. The detection of Ag^+ in river water samples

The portability of the PAAm hydrogel film and the label-free capability of the LC droplet-based sensor make the sensing strategy proposed here highly promising for practical applications. Therefore, we investigated the response ability of the LC droplet-based sensor to spiked river water samples. As depicted in Fig. 7c, LC droplets anchored with C10–M–C remain in a radial configuration during the PAAm hydrogel was immersed in river water taken from the Xiangjiang River, indicating that the river water does not affect the adsorption of C10–M–C and the configuration of LC droplets. While LC droplets underwent a configurational transition when the PAAm hydrogel was immersed in river water containing 1 μM Ag^+ as seen in Fig. 7d. By equipping a portable microscope lens on a smartphone and placing the LC droplets between two orthogonally oriented polarizers (Figure S4), we were able to capture polarized microscopy images of the LC droplets using the smartphone. As shown in Fig. 7 e and f, the obtained microscopic images clearly depict the changes in the configurations. Therefore, compared to other methods as shown in Table 1, we have achieved both portable detection and high sensitivity. This capability empowers our LC droplet-sensor with the ability for portable, real-time and on-site analysis of environmental samples.

4. Conclusion

In conclusion, we have modified cytidine with *n*-decyl alcohol through an enzymatic acylation. The successfully synthesis of C10–M–C was confirmed by FT-IR and ^1H NMR spectrum. After demonstrating the surfactant properties of C10–M–C, it was used to anchor onto the surface of LC droplets to adjust the configuration of LC droplets. Moreover, the C10–M–C on the surface of LC droplets exhibited excellent absorption stability to acids and bases, as evidenced by no change in the configuration of LC droplets. Upon introduction of Ag^+ into the solution, the configuration of LC droplets transformed, indicating the potential of C10–M–C−anchored LC droplets for use as an Ag^+ sensor. The LC droplet-based sensor was found to respond to Ag^+ as low as 0.6 μM, making it suitable for the detection of Ag^+ in environmental and food samples. By equipping a portable microscope lens on a smartphone and placing the LC droplets between two orthogonally oriented polarizers, the sensor enables the monitoring of Ag^+ in river water for potential human health hazards using a smartphone. This indicates that the LC droplet-based sensor proposed here can be applied for reliable, rapid, sensitive, and portable detection of Ag^+.

CRediT authorship contribution statement

Guannan Zhang: Methodology, Investigation, Formal analysis, Data curation, Writing – original draft, Writing – review & editing. **Wenting Zhao:** Investigation, Formal analysis, Data curation, Writing – review & editing. **Wenzhao Liu:** Formal analysis, Investigation. **Jun Zhou:** Resources, Writing – original draft, Writing – review & editing. **Zhaoyang Wu:** Resources, Writing – original draft, Supervision, Project administration, Writing – review & editing.

Declaration of Competing Interest

The authors declare that they have no known competing financial interests or personal relationships that could have appeared to influence the work reported in this paper.

Data availability

Data will be made available on request.

Acknowledgments

This study was financially supported by the National Natural Science Foundation of China (22174040 and 21874037).

Appendix A. Supplementary material

Supplementary data to this article can be found online at https://doi.org/10.1016/j.jcis.2023.06.111.

References

[1] J.L. Barriada, A.D. Tappin, E.H. Evans, E.P. Achterberg, Dissolved silver measurements in seawater, TrAC Trends Anal. Chem. 26 (8) (2007) 809–817.
[2] Y.-H. Lin, W.-L. Tseng, Highly sensitive and selective detection of silver ions and silver nanoparticles in aqueous solution using an oligonucleotide-based fluorogenic probe, Chem. Commun. 43 (2009) 6619–6621.
[3] R. Freeman, T. Finder, I. Willner, Multiplexed Analysis of Hg2+ and Ag+ Ions by Nucleic Acid Functionalized CdSe/ZnS Quantum Dots and Their Use for Logic Gate Operations, Angew. Chem. Int. Ed. 48 (42) (2009) 7818–7821.
[4] S. Choi, G. Lee, I.S. Park, M. Son, W. Kim, H. Lee, S.-Y. Lee, S. Na, D.S. Yoon, R. Bashir, J. Park, S.W. Lee, Detection of Silver Ions Using Dielectrophoretic Tweezers-Based Force Spectroscopy, Anal. Chem. 88 (22) (2016) 10867–10875.
[5] I.M. Rust, J.M. Goran, K.J. Stevenson, Amperometric Detection of Aqueous Silver Ions by Inhibition of Glucose Oxidase Immobilized on Nitrogen-Doped Carbon Nanotube Electrodes, Anal. Chem. 87 (14) (2015) 7250–7257.
[6] T. Li, L. Shi, E. Wang, S. Dong, Silver-Ion-Mediated DNAzyme Switch for the Ultrasensitive and Selective Colorimetric Detection of Aqueous Ag+ and Cysteine, Chem. Eur. J. 15 (14) (2009) 3347–3350.
[7] B. Li, Y. Du, S. Dong, DNA based gold nanoparticles colorimetric sensors for sensitive and selective detection of Ag(I) ions, Anal. Chim. Acta 644 (1) (2009) 78–82.
[8] Y. Wen, F. Xing, S. He, S. Song, L. Wang, Y. Long, D. Li, C. Fan, A graphene-based fluorescent nanoprobe for silver(i) ions detection by using graphene oxide and a silver-specific oligonucleotide, Chem. Commun. 46 (15) (2010) 2596–2598.
[9] D.S. Miller, R.J. Carlton, P.C. Mushenheim, N.L. Abbott, Introduction to optical methods for characterizing liquid crystals at interfaces, Langmuir 29 (10) (2013) 3154–3169.
[10] S. Setia, S. Sidiq, J. De, I. Pani, S.K. Pal, Applications of liquid crystals in biosensing and organic light-emitting devices: future aspects, Liq. Cryst. 43 (13–15) (2016) 2009–2050.
[11] I. Verma, S. Sidiq, S.K. Pal, Detection of creatinine using surface-driven ordering transitions of liquid crystals, Liq. Cryst. 43 (8) (2016) 1126–1134.
[12] L. Zhou, Q. Kang, M. Fang, L. Yu, Label-free, rapid, and sensitive detection of carboxylesterase using surfactant-doped liquid crystal sensor, J. Mol. Liq. 296 (2019), 111921.
[13] S. Wang, Y. Qi, Q. Chen, G. Zhang, B. Liu, F. Xiao, J. Zhou, Z. Wu, R. Yu, Control of Liquid Crystal Microarray Optical Signals Using a Microspectral Mode Based on Photonic Crystal Structures, Anal. Chem. 93 (34) (2021) 11887–11895.

[14] I.H. Lin, D.S. Miller, P.J. Bertics, C.J. Murphy, J.J. de Pablo, N.L. Abbott, Endotoxin-induced structural transformations in liquid crystalline droplets, Science 332 (6035) (2011) 1297–1300.
[15] D.S. Miller, X. Wang, J. Buchen, O.D. Lavrentovich, N.L. Abbott, Analysis of the internal configurations of droplets of liquid crystal using flow cytometry, Anal. Chem. 85 (21) (2013) 10296–10303.
[16] J. Deng, W. Liang, J. Fang, Liquid Crystal Droplet-Embedded Biopolymer Hydrogel Sheets for Biosensor Applications, ACS Appl. Mater. Interfaces 8 (6) (2016) 3928–3932.
[17] O.D. Lavrentovich, Topological defects in dispersed words and worlds around liquid crystals, or liquid crystal drops, Liq. Cryst. 24 (1) (1998) 117–126.
[18] D.S. Miller, X. Wang, N.L. Abbott, Design of Functional Materials based on Liquid Crystalline Droplets, Chem. Mater. 26 (1) (2014) 496–506.
[19] I. Verma, S. Sidiq, S.K. Pal, Protein triggered ordering transitions in poly (L-lysine)-coated liquid crystal emulsion droplets, Liq. Cryst. 46 (9) (2019) 1318–1326.
[20] S. Sidiq, G. Prasad, A. Mukhopadhaya, S.K. Pal, Poly(l-lysine)-Coated Liquid Crystal Droplets for Cell-Based Sensing Applications, J. Phys. Chem. B 121 (16) (2017) 4247–4256.
[21] T. Bera, J. Deng, J. Fang, Protein-induced configuration transitions of polyelectrolyte-modified liquid crystal droplets, J. Phys. Chem. B 118 (18) (2014) 4970–4975.
[22] T. Bera, J.Y. Fang, Polyelectrolyte-coated liquid crystal droplets for detecting charged macromolecules, J. Mater. Chem. 22 (14) (2012) 6807–6812.
[23] W. Li, M. Khan, L. Lin, Q. Zhang, S. Feng, Z. Wu, J.M. Lin, Monitoring H2O2 on the Surface of Single Cells with Liquid Crystal Elastomer Microspheres, Angew. Chem. Int. Ed Engl 59 (24) (2020) 9282–9287.
[24] B.J. Ortiz, M.E. Boursier, K.L. Barrett, D.E. Manson, D. Amador-Noguez, N. L. Abbott, H.E. Blackwell, D.M. Lynn, Liquid Crystal Emulsions That Intercept and Report on Bacterial Quorum Sensing, ACS Appl. Mater. Interfaces 12 (26) (2020) 29056–29065.
[25] A. Dan, P. Agnihotri, M. Brugnoni, E. Siemes, D. Woll, J.J. Crassous, W. Richtering, Microgel-stabilized liquid crystal emulsions enable an analyte-induced ordering transition, Chem. Commun. 55 (50) (2019) 7255–7258.
[26] W. Pu, H. Zhao, C. Huang, L. Wu, D. Xua, Fluorescent detection of silver(I) and cysteine using SYBR Green I and a silver(I)-specific oligonucleotide, Microchim. Acta 177 (1) (2012) 137–144.
[27] F.M. Menger, S.A.A. Rizvi, Relationship between Surface Tension and Surface Coverage, Langmuir 27 (23) (2011) 13975–13977.
[28] A. Sokołowski, A. Bieniecki, K.A. Wilk, B. Burczyk, Surface activity and micelle formation of chemodegradable cationic surfactants containing the 1,3-dioxolane moiety, Colloids Surf. A Physicochem. Eng. Asp. 98 (1) (1995) 73–82.
[29] X.-F. Li, Z.-H. Lu, G.-L. Zhao, H. Wu, Y.-G. Yu, A facile whole-cell biocatalytic approach to regioselective synthesis of monoacylated 1-β-d-arabinofuranosylcytosine: Influence of organic solvents, Bioresour. Technol. 114 (2012) 6–11.
[30] J.T. Davies, E.K. Rideal, Interfacial Phenomena, Science 134 (3490) (1961) 1611–1612.
[31] G. Zhang, A. Zhu, S. Wang, Q. Chen, B. Liu, J. Zhou, Z. Wu, Stabilizing liquid crystal droplets with hydrogel films and its application in monitoring adenosine triphosphate, Colloids Surf. A Physicochem. Eng. Asp. 654 (2022) 130122.
[32] Y. Xu, Y. Chang, Y. Yao, M. Zhang, R.L. Dupont, A.M. Rather, X. Bao, X. Wang, Modularizable Liquid-Crystal-Based Open Surfaces Enable Programmable Chemical Transport and Feeding using Liquid Droplets, Adv. Mater. 34 (20) (2022) e2108788.
[33] J.-C. Jin, B.-B. Wang, Z.-Q. Xu, X.-H. He, H.-F. Zou, Q.-Q. Yang, F.-L. Jiang, Y. Liu, A novel method for the detection of silver ions with carbon dots: Excellent selectivity, fast response, low detection limit and good applicability, Sensors Actuators B-Chem. 267 (2018) 627–635.
[34] J.-G. Liang, X.-P. Ai, Z.-K. He, D.-W. Pang, Functionalized CdSe quantum dots as selective silver ion chemodosimeter, Analyst 129 (7) (2004) 619–622.
[35] Z. Wang, J. Zhao, Z. Li, J. Bao, Z. Dai, Sequence and Structure Dual-Dependent Interaction between Small Molecules and DNA for the Detection of Residual Silver Ions in As-Prepared Silver Nanomaterials, Anal. Chem. 89 (12) (2017) 6815–6820.
[36] X. Gao, Y. Lu, R. Zhang, S. He, J. Ju, M. Liu, L. Li, W. Chen, One-pot synthesis of carbon nanodots for fluorescence turn-on detection of Ag+ based on the Ag+-induced enhancement of fluorescence, J. Mater. Chem. C 3 (10) (2015) 2302–2309.
[37] B. Liu, H. Tan, Y. Chen, Visual detection of silver(I) ions by a chromogenic reaction catalyzed by gold nanoparticles, Microchim. Acta 180 (5) (2013) 331–339.